Superconducting joints of melt textured $YBa_2Cu_3O_{7-\delta}$ monoliths: preparation, microstructure and critical currents.

Adriana Simona Iliescu

February 1, 2005

Agradecimientos

Con estas palabras quiero expresar mi más sincero agradecimiento a todas aquellas personas que de una forma u otra me han ayudado a avanzar por el camino que a recorrido esta tesís y en especial: Al Profesor Xavier Obradors y a la Doctora Teresa Puig, directores de esta tesís, por haberme dado la oportunidad de formar parte de este proyecto de investigación y por todo el tiempo y el apoyo que me han dedicado.

Al Doctor Xavier Granados, por su paciencia en atender a todas mis preguntas en todo momento y su ayuda en realizar mi trabajo experimental.

A Dr. Miquel Carrera y Dr. Jaume Amoros por haberme facilitado el acceso al metodo "Caragol" utilizado en esta tesís para el calculo de densidades de corrientes críticas.

A la empresa "Nexans Superconductors" y al laboratorio "IPHT", Jena por haberme proporcionado las muestras de partida utilizadas en esta tesís.

A Dr. Jan Evetts por su colaboración en la puesta en marcha de la methodologia desarrollada en este trabajo.

A Anna Palau por la colaboración en el desarrollo de la metodologia utilizada en esta tesis para el calculo de corrientes criticas de las uniones superconductoras.

A Anna Esther Carrillo por su ayuda en el analisis microestructural de las uniones mediante microscopia electronica de barrido.

A Dr. Simon Sena por su importanmte colaboración en la puesta en marcha del sistema de magnetometria Hall.

A todos los miembros del grupo y compañeros por todo el apoyo y la alegría que me han dado durantes estos años, y especialmente a JC, Neus, Andrea, Diego, Anna, Joffre, Oscar, Irene, David.

Quiero agradecer al proyecto de la Comunidad Europea "Supermachines", IHP-RTN-99-1, "Advanced Rotating Electrical Machines Exploiting High Tem-

peratures Superconducting Components" por su financiación. Tambien, mi agradecimientos a toda la gente involucrada en este proyecto (Bernat, Elena, etc) por hacer más facil y más divertido el desplazamiento a las reuniones de proyecto.

A Trini y a Vicente por su constante ayuda en los tramites burocraticos.

A Lamya, Daciana y Martí por su sincera amistad.

Pero, ante todo a mis padres y a mi hermano Catalin por todo su apoyo, por su querer incondicionado, desde aquí...va multumesc si va iubesc mult de tot!

Dedicada a Martín

Contents

Chapter 1

Aim, background and working plan

In 1911 the Dutch physicist, Heike Kamerlingh Onnes, discovered in his laboratory in Leiden that the dc resistivity of mercury suddenly drops to zero whenever the sample is cooled below 4.2K, the boiling point of liquid helium. He named the new phenomena - superconductivity. In the years to follow it was discovered that many other metallic elements exhibit superconductivity at very low temperatures. Unfortunately, the industrial applications of those "low-critical temperature" superconductors was restricted by the cost of the liquid helium and the complicated operation of the cooling system. Since then many efforts have been made in order to discover materials which have higher critical temperature (T_c). In late 1986, G.Bednorz and K.A.Muller, researchers in IBM Laboratory, discovered superconductivity in cuprate oxides. More precisely, they found evidence for superconductivity at about 30K in LaBaCuO ceramics. In February 1987 a research group in Alabama and Houston, coordinated by W. Lu and P. Chu, discovered superconductivity in $YBa_2Cu_3O_{7-\delta}$ ceramics. Its T_c was about 90K. This was the existence of a superconductor with a critical temperature above that of liquid nitrogen which is a much cheaper coolant then the liquid helium. Only a year later $Bi_2Sr_2Ca_2Cu_3O_{10}$, $Tl_2Ba_2Ca_2Cu_3O_{10}$ and $HgBa_2Ca_2Cu_3O_8$ cuprate oxides were discovered with $T_c \simeq$110K, $T_c \simeq$120K and $T_c \simeq$134K respectively. Thus, a new class of materials, cooper oxide ceramics

with a layered perovskite structure had rapidly arisen.

However, T_c is not the only factor to be considered and most applications require large critical current densities (J_c) in the presence of large magnetic fields. Large $REBa_2Cu_3O_7$ monoliths, where RE is Rare Earth (i.e Tm, Yb, Er), have significant potential for technical applications, since they can trap fields which are greater than the conventional permanent magnets. The field trapping capability of bulk superconductors is dependent on the critical current density J_c and the size of the bulk free of weak-links. Thus, an enlargement of grain size is important along with an increase in the values of J_c.

In recent years, a strong effort has been devoted to develop methodologies to enlarge the dimensions of biaxially textured $YBa_2Cu_3O_{7-\delta}$ monoliths and fabricate complex shapes. Melt texturing of $YBa_2Cu_3O_{7-\delta}$ [1] has emerged as a unique technique for the preparation of bulk superconducting materials free of grain boundaries. Currently, the most common melt process technique used for the fabrication of $YBa_2Cu_3O_{7-\delta}$ monoliths is based on Top Seeded Melt Growth (TSMG) [1, 2] in which a small single crystal with lattice parameters similar to that of YBCO material is used as a seed by placing it on the top surface of a YBCO compacted pellet to provide a homogeneous grain nucleation site.

Small single domain samples of $YBa_2Cu_3O_{7-\delta}$ can be rapidly fabricated, with high yield, using this method. Unfortunately, the TSMG process is limited by the difficulty of producing larger components of complex geometries that are required for magnetic levitation systems, motors, rotors and current limitation elements.

General Aim

The aim of this PhD thesis has been to develop a technology which would be able to achieve superconducting pieces of large dimensions and complex geometries for its integration into different superconducting dispositives based on fabricating superconducting joints.

Thus, the final goal of this work is to obtain $YBa_2Cu_3O_{7-\delta}$ samples with different geometries and bigger dimensions than those obtained by the crystalline growth techniques. This need has driven our investigation to welding techniques that can joint two or more $YBa_2Cu_3O_{7-\delta}$ single-domains by a solidification process using welding agents whose melting points are below the melting point of $YBa_2Cu_3O_{7-\delta}$ material. The welding agents used in this work were based on Ag:

1. Ag_2O powder by suspension;

2. Ag thin foil;

Figure 1.1 shows several typical configurations of assemblies to be joined, where the starting single crystal pieces and the welding agent are indicated. As it can be seen in figure 1.1, the starting tiles should be cut to have the desired final shape (i.e. ring, bar, parallelepiped, etc.) and then, the Ag-based welding agent should be inserted between the two YBCO surfaces to be joined. As it can be seen in figure 1.1, the welded interface can correspond actually to different crystallographic planes of the single crystal YBCO tiles. In figure 1.1a the welded surface is parallel to the c-axis of the YBCO structure while in figure 1.1b the welded surface is perpendicular to the c-axis. Finally, in figure 1.1c the different YBCO tiles can have either the c-axis parallel or with a radial structure, i.e. the c-axes are directed in all the tiles towards the center of the ring structure. The advantage of any of these different configurations will require a detailed study in each case, but, it will be mainly determined by the desired performances of the assembly in the corresponding device.

Background

The need to improve the superconducting properties of $YBa_2Cu_3O_{7-\delta}$ material has driven the scientists to study the influence of different additives on the YBCO material properties. Several authors have tried to add silver into the $YBa_2Cu_3O_{7-\delta}$ matrix and, afterwards, by top seeding grown melt textured

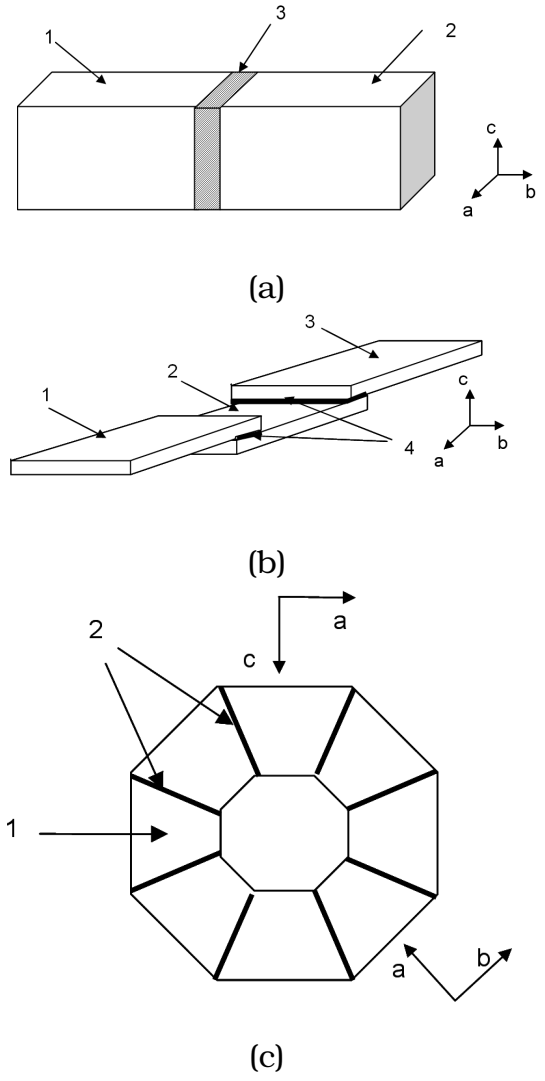

Figure 1.1: Schematic drawing of the localization of the Ag based welding material and orientation of the YBCO single crystalline ceramic tiles. (a) Two pieces of YBCO having the same crystallographic orientation, 1 and 2, are joined by the Ag based welding materials, 3. The joined interface is parallel to the c-axis. (b) Three pieces of YBCO having the same crystallographic orientation, 1, 2 and 3 are joined by Ag based welding material, indicated by 4, in such a way that the joined interface is perpendicular to the c-axis. (c) Ring-shaped configuration where the individual YBCO elements (1) can have different crystallographic orientations. In one case the c-axis points towards the central part of the ring and in the second configuration all the c-axis of the elements are parallel and directed perpendicular to the ring. The silver based materials are also indicated (2).

YBCO/Ag composites. Differential thermal analysis have demonstrated a decrease of the peritectic temperature by 40°C for Ag_2O admixtures above 5wt%

[3, 4, 5]. In reference [5] the composition used was:

$$(0.7MY123 + 0.3MY211 + 0.06MCeO_2) + xwt\%Ag_2O \tag{1.1}$$

where $5 < x < 20$.

A silver addition to $YBa_2Cu_3O_{7-\delta}$ composition was found to be very effective for the improvement of the mechanical properties of the pellets. This lies in the fact that the mean distance separation between the microcracks lying parallel to the ab planes has been strongly reduced [5]. Additionally, a reduction of the porosity, normally encountered in the $YBa_2Cu_3O_{7-\delta}$ samples obtained by TSMG method, was observed by optical microscopy. As a consequence, an important improvement of critical current density was appreciated, which in samples with 20wt%Ag_2O at 77K could reach 70% at 0T.

Unfortunately, this method shows the same limitations as the TSMG process used to obtain $YBa_2Cu_3O_{7-\delta}$ single-domains free of additives. Even if the superconducting and mechanical properties have been improved, the obtention of larger and complex shaped samples is considered a major difficulty.

One solution to overcome all these problems is to succeed in welding several well-orientated $YBa_2Cu_3O_{7-\delta}$ textured domains. A number of approaches, to obtain joints capable of transporting supercurrents with high critical current densities have been used with various degrees of success. These approaches can be divided into three main categories:

1. natural joining during multi-seeded melt growth of a single green body *(multiseeding)*;

2. direct contact joining which might include pressure weighting of the joint *(direct contact)*;

3. joining using a high-T_c filler material that has a decomposition temperature lower than that of the parts to be joint *(artificial joining)*.

A method developed in order to achieve big monoliths with complex shapes such as rings was that of multiseeding. The basic concept of multiseeding is to place several seeds with similar crystallographic orientation on the top surface of a just compacted YBCO material (green body) [6, 7]. These authors have used Sm123 seeds and the c-direction of the seeds was normal to the top surface of the YBCO block. By this technique, the processing time was reduced. However, the main difficulty in the use of multiple seeds is that usually impurities remain at the joint interfaces which lead to poor superconducting connectivity of the grains. Thus, the critical current density across the joint is drastically reduced.

The idea to weld two or more YBCO single crystals has been considered by several authors as a promising alternative for the production of large scale monoliths with complex shapes [8, 9, 10, 11, 12, 13, 14, 15]. The methods described up to now are based on the use of welding agents based on Rare Earth (RE) like: Tm123, Yb123, Er123 [8, 11, 13, 14, 16]. In general, the decomposition temperature of a solder material must be lower than that of the mother blocks. In addition, its superconducting properties should be similar or superior to those of mother blocks. If the solder material has poor superconducting properties, supercurrent flow will be interrupted at the joined region. In all these cases, the welding is achieved through a slow cooling process of the molten solder which solidifies epitaxially on the adjacent YBCO single domains.

In this way, Zheng *et al.* [11] have used a spacer material consisting of Tm123 with a 25wt% admix of Y211. The peritectic decomposition of the Tm123/Y211 mixture is about 995°C, $\sim$ 20°C below that of the YBCO parts which makes it suitable as a solder material. Walter *et al.* have used as welding material a layer of Er123+25mol% Er_2O_3 and Delamare *et al.* [17] have used a 1mm-thickness of Yb123 powder.

Unfortunately, these techniques display limitations that inhibit their use on a large scale. The main problems found in these methods are:

1. Some phase segregation, like $BaCuO_2$ and RE211 (i.e. Yb211, Tm211,

Y211), and residual porosities are encountered at the YBCO/YBCO interface. Non-superconducting phases deposited at the YBCO interface produce weak links that can severely limit the superconducting transport across the joint. Such behavior has been demonstrated using magneto-optical imaging [11, 16] and transport current measurements [10].

2. Excessive mismatch between lattice parameters of the matrix and the joining material can lead to the formation of micro and macrocracks which limit the critical current density of the final joints.

3. Some joining compositions, i.e Yb123, display a lower T_c and hence lower J_c at 77K than the material to be welded.

Recently, K. Iida *et al.* [18] tried to join relatively large YBCO/Ag blocks using an ErBCO/Ag solder. It has been demonstrated that Ag addition to YBCO matrix improve the superconducting and mechanical properties of this material [5]. Additionally, ErBCO/Ag material has a peritectic temperature T_p∼951°C), thus lower than the melting point of YBCO/Ag composites, and exhibits similar superconducting properties to the material to be joint. K. Iida *et al.* have found that the superconducting properties of the joint could be improved by controlling the Er211 content in the solder.

Other welding alternatives, where no external welding agent is employed (direct contact), have been proposed [8, 19]. Salama *et al.* [8] used an uniaxial pressure and temperatures less than 930°C to join two polished YBCO surfaces by a solid state diffusion process. This technique relies on a perfect contact between both surfaces before joining which is rarely achievable, since no evidence of melting was reported during the joining process. The method proposed by L. Chen *et al.* [19] consists on welding bulk YBCO materials by using a superheating effect, i.e. to melt all the surfaces of the tiles, particulary that to be welded, while the bulk remains solid. The thermal process has been carried out in oxygen atmosphere under a pressure of 1atm. This process has been demonstrated

to lead to good quality joints.

Bradley *et al.* [20] proposed another technique based on a direct contact. Polished YBCO were joined at temperatures between 920°C-1000°C under an uniaxial pressure of 0.5MPa to ensure that a firm contact was achieved between the joining parts. In this case the interfacial melting is generated by trapped $BaCuO_2 - CuO$ flux remaining in the bulk of melt processed YBCO. Microstructural analysis have shown that the interface contains some regions of amorphous liquid phase and a misorientation angle spanning between 2° and 4° which can be possible sources of J_c reduction.

Unfortunately, direct contact methods require a very tight control of temperature gradients in the furnace and the welding process is dependent on the starting microstructure of YBCO tiles. Thus, a scale-up of this process might not be very suitable.

An improvement of the microstructure and superconducting properties of YBCO monoltiths was demonstrated by Puig *et al.* [12] by using a solid YBCO/Ag composite cut from a large top seeding melt textured grown grain with a reduced peritectic temperature compared to YBCO to weld two grains together. They have used the following composition of this agent:

$$(0.7MY123 + 0.3MY211) + 15wt\%Ag_2O \tag{1.2}$$

The composition displays similar properties and, hence, is suitable for high quality joining. This welding agent was used in bulk form prepared as described previously [5]. By optical microscopy they have observed that no secondary phases or voids exist at the interface. It was also observed that the Ag particles, having a typical size between 10 and 50 microns, remain confined within the welding volume. Thus, a sharp interface was defined. It was remarkable that the residual porosity at the YBCO/Ag interface had been almost eliminated. The superconducting properties of the melt processed ceramic, studied by means of magneto-optical imaging and trapped field measurements, were even better than

the initial YBCO tiles [12].

This method has overcome the limitations that other techniques showed, which means that the secondary phases and the porosity existent at the YBCO/YBCO interface have been eliminated. The experimental difficulty was that YBCO/Ag single domains should be first prepared in a separate process and this is usually difficult to prepare in large dimensions.

As a consequence, observing that the addition of Ag into YBCO matrix has improved the mechanical and superconducting properties of the material and that the major problem of this method is the difficulty in achieving a complex geometry, in this thesis we have tried to go beyond this state of the art by developing another technique which still uses welding agents based on Ag.

The welding process between two YBCO single-domains described in this thesis is based on the knowledge of high-T_c phase diagram of YBCO-x%Ag system. It is known that when x is between 5-20wt%, the peritectic temperature is reduced, enabling, thus, an interfacial melting of the YBCO blocks by introducing Ag close to the interface and inducing their diffusion to the bulk interface. The temperature to which the interfacial melting takes place will be lower than that of the bulk YBCO and the homogeneity in temperature for scaling-up the process to industrial applications will not be so restricted. The difference with the technique proposed by L.Chen *et al.* [19] is that it does not require YBCO melting of all the YBCO surfaces, but only that in contact with Ag. Additionally, the difference between the melting point of the interface and the YBCO material is larger than ~ 40°C.

Specific Aims

The general goal of this PhD thesis was to develop a technology necessary to obtain large and complex shaped YBCO melt textured samples for their use in applications like rotors for motors, systems based on levitation, fault current limiters, etc. In this way several specific objectives have been established:

1. Find a suitable welding material for the welding process;
2. Optimize the welding process by studying the influence of different parameters such as: Ag thickness (g_{Ag}), processing temperature (T_{max}), melting time (t_{melt}), welding architecture, cooling rate (r) and window temperature (ΔT);
3. Obtain an homogeneous microstructure of the final joints and analyze it with scanning electronic microscopy (SEM) and optical microscopy;
4. Optimize the oxygen content of the final joints to establish the superconducting behavior;
5. Determine the trapped magnetic field capacity of the samples obtained using an in-field Hall Probe imaging system;
6. Determine the critical current densities of both, starting material and YBCO/Ag/YBCO joints from trapped magnetic field measurements ;
7. Develop a scalable technique which permits us to obtain the critical current density from the trapped magnetic field measurements;
8. Obtain the critical current density of the final joints in the 80-100% range of that of the starting YBCO tiles by optimizing the different parameters of the welding process.

Working Plan

Figure 1.2 shows the working plan followed to achieve all the objectives stated in this PhD thesis.

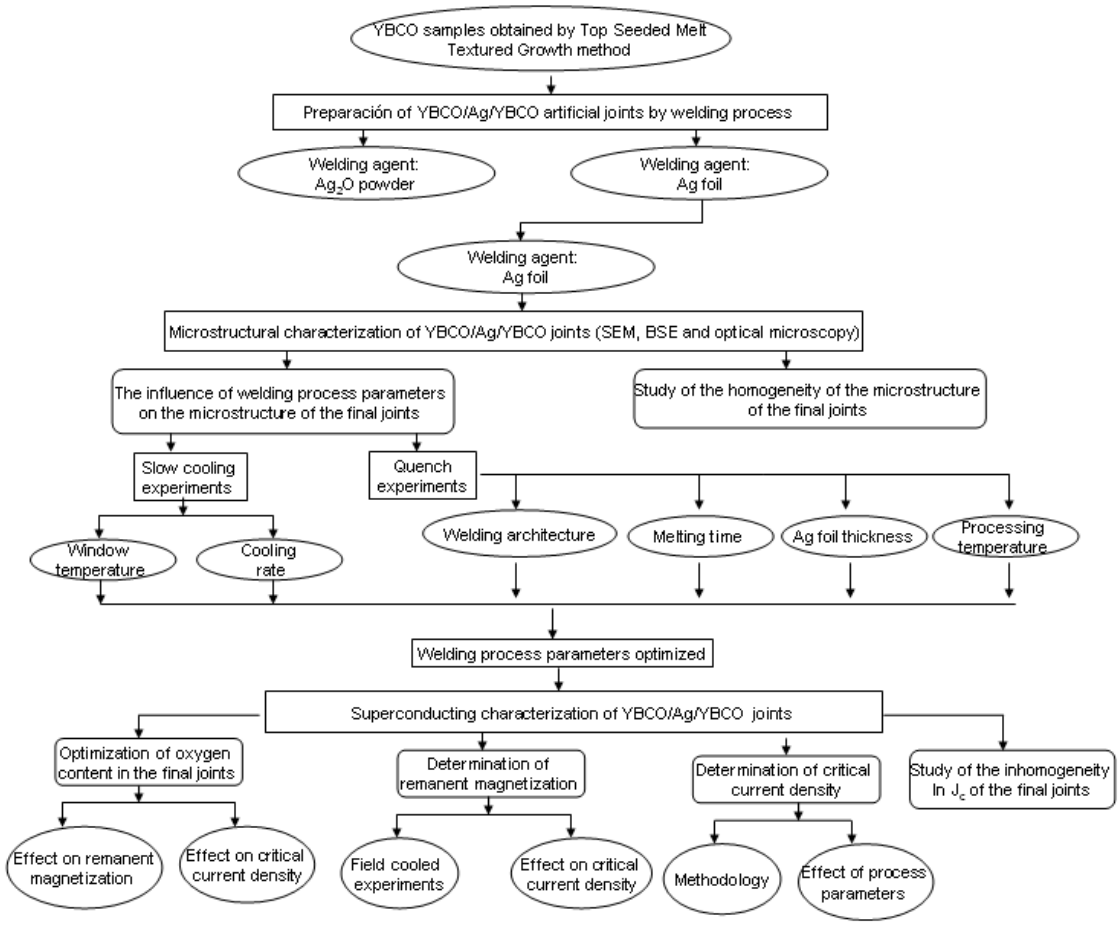

Figure 1.2: Working plan followed in this PhD thesis.

Chapter 2

Introduction

2.1 General remarks

For a material to be considered a superconductor it has to exhibit two distinctive properties:

1. The electrical resistivity in superconductors is zero for temperatures below a certain temperature called critical temperature (T_c) (figure 2.1a). So, one can apply dc electrical current without losses. In normal conducting materials the existence of resistivity is related to the existence of scattering between the carriers with impurities. However, in superconductors, the carriers are coupled forming Cooper pairs which are not scattered and therefore, zero resistance is obtained. The condensate that results from this coupling is represented by a wave function (Ψ) that varies in distances given by the coherence length ($\xi(T)$).

2. The applied magnetic field is completely expelled from the interior of the superconducting specimen at temperatures below the critical temperature (T_c). The expulsion is generated by Cooper pairs circulating at the surface of the sample, that are able to screen the external magnetic field. These currents penetrate into the sample in a distance characterized by the penetration length, $\lambda(T)$, leading to an exponential decay of the magnetic field. The complete expulsion of the magnetic field from the interior of a super-

conducting sample is known as the Meissner-Ochsenfeld Effect which is represented in figure 2.1b.

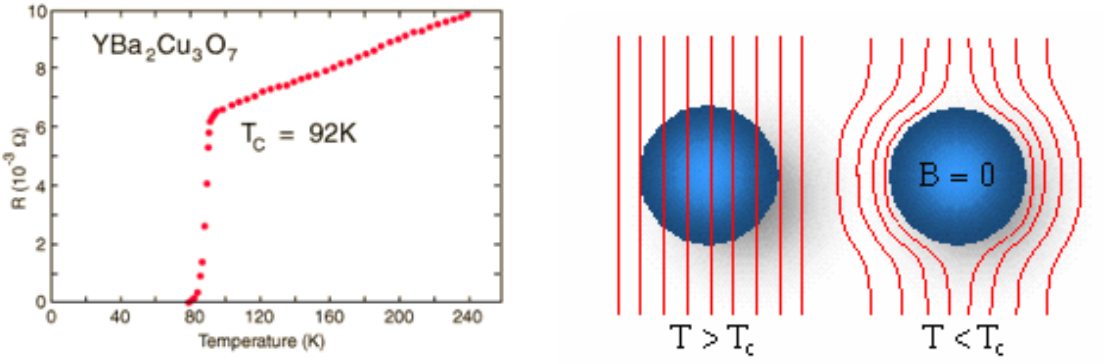

(a) (b)

Figure 2.1: a) Temperature dependence of electrical resistivity of the oxide superconductor $YBa_2Cu_3O_{7-\delta}$; b) Expulsion of a weak, external magnetic field from the interior of the superconducting material.

Superconductors are of two types: type I and type II superconductors, whether the Ginzburg-Landau parameter k is smaller or larger than $1/\sqrt{1/2}$, respectively. The Ginzburg-Landau parameter k is defined as:

$$k = \frac{\lambda}{\xi} \tag{2.1}$$

where λ describes the penetration depth of the magnetic field inside the superconductor and ξ is the characteristic length over which the Cooper pair density increases from 0 to its maximum value n. For a type I superconductor $k < 1/\sqrt{1/2}$, whereas for a type II superconductor $k > 1/\sqrt{1/2}$.

2.1.1 Type I superconductors

Type I superconductor possesses only one critical magnetic field $H_c(T)$, below which the superconductor produces shielding currents that flow on the surface of the material expelling the magnetic field from its interior (see figure 2.2a). In this situation, the superconductor is in the Meissner state. Above H_c the applied

magnetic field penetrates completely into the interior of the material, disrupting the superconductivity.

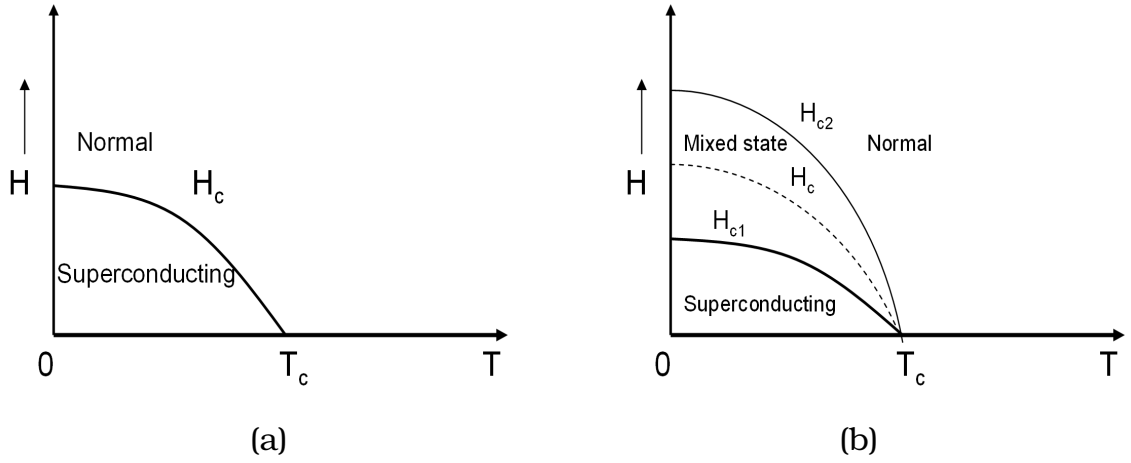

Figure 2.2: Magnetic phase diagram (H(T)) for: a) Type I superconductors: one critical field H_c exists; b) Type II superconductors: where two critical fields exist (lower critical field (H_{c1}) and upper critical field (H_{c2})).

2.1.2 Type II superconductors

Type II superconductors are characterized by two critical fields: a lower critical field, H_{c1}, and an upper critical field, H_{c2}. Figure 2.2b shows the magnetic phase diagram for a type II superconductor. Below H_{c1}, the superconductor behaves like a type I superconductor and it is in the Meissner state, Meissner currents flowing at the surface disabling the magnetic field to penetrate into the sample. As the magnetic field is increased above H_{c1}(T) but still below the H_{c2}, the magnetic field penetrates the superconductor in the form of tiny quantized microscopic filaments called vortex [21]. A vortex consists of a normal core where the cooper pair density is zero and this core is surrounded by a superconducting region in which flows a persistent supercurrent. Further increasing the magnetic field, the number of vortices inside the sample increases and at the upper critical field H_{c2}, the cores of the neighboring vortex overlap and the sample goes to the normal state.

Between H_{c1} and H_{c2} the superconductor is said to be in the mixed state. A schematic representation of the penetration of these flux lines (vortex) inside the sample, is shown in figure 2.3. In this state, the vortices are arranged forming an hexagonal lattice with a lattice parameter a_0 depending on B as follows:

$$a_0 = \sqrt{\frac{\phi_0}{B}} \tag{2.2}$$

where ϕ_0 is the is the flux quantum that each individual vortex is carrying, and has value of ϕ_0=h/2e=2.07 $\times$ 10^{-15} Wb. In this case h is the Planck constant and e is the charge of electron.

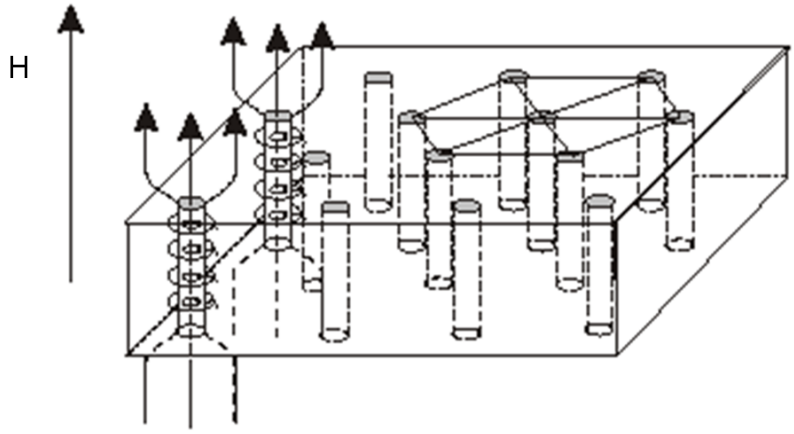

Figure 2.3: Representation of the mixed state, where each vortex is surrounded by shielding currents.

2.1.3 Critical current density

The critical current density is the most important property that describes a superconductor from the point of view of technical applications. It corresponds to the maximum current which can transport the material without dissipation.

In the mixed state, there are vortices in the material. When an external current density $\overrightarrow{j}$ flows along a superconducting sample which is in the mixed state, the flux lines start to move under the action of the Lorentz force ($\overrightarrow{F_L}$= $\overrightarrow{j} \times \overrightarrow{B}$). The movement of flux lines causes the appearance of voltage. When the flux moves at the velocity of $\overrightarrow{v}$, an electric field $\overrightarrow{E}$ is created in the direction of the current as $\overrightarrow{E} = \overrightarrow{v} \times \overrightarrow{B}$ giving rise to ohmic losses. In this situation, the desired superconducting property of dissipation free-current flow is lost. In order to recover it, the flux lines have to be fixed to pinning centers in such a way that $\overrightarrow{v}$=0. The force that holds the core of the flux lines at the pinning centers is called pinning force (F_p) and it allows the system to sustain the Lorentz force between the flux lines and the current without flux motion and dissipation. If the Lorentz force equals the F_p, the depinning critical current density j_{dp} is achieved and the flux lines start to move producing dissipation. In conventional type II superconductors, the critical current density can be associated to j_{dp}.

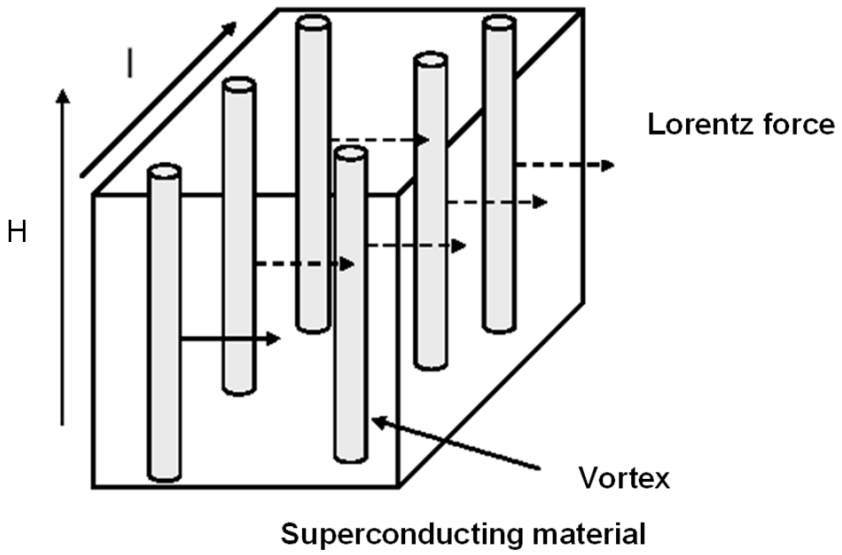

Figure 2.4: The Lorentz force F_L on flux lines in the presence of the current.

Pinning centers in a superconductor result from structural inhomogeneities in the material that yield a local reduction in the order parameter. Therefore, the vortex can reduce its energy when positioned on a pinning center. Thus, a superconductor free of defects, in the mixed state, has a critical current density J_c =0. Pinning centers should be on the scale of the coherence length ξ to be effective, i.e. in the nanometer range in the case of high-T_c superconductors. Typical pinning centers found in high temperature superconductor materials are: twin boundaries, stacking faults, dislocations, oxygen vacancies.

The critical current density of oxide superconductors, as in the case of conventional superconductors, depends on the applied magnetic field and temperature at which is measured. By increasing the temperature and the applied magnetic field, the critical current density diminishes. In addition, high-T_c superconductors are highly anisotropic, thus the critical current density depends on the crystallographic direction in which is applied.

Critical state model

The critical current density can be estimated by using the critical state model. The basic concept of this model is that an irreversible superconductor can carry a limiting macroscopic superconducting current density, i.e J_c. The model assumes that penetrated supercurrents flow with a density equal to the critical current density. The critical current density, J_c is related to the magnetic induction value, B, at each point.

In the simplest critical state approximation, the spatial gradient of H or J_c is assumed to be constant inside the sample and it is called Bean model [22]. In a real case, J_c is dependent on B, and therefore J_c is not constant anymore inside the superconductor. However, it has been shown that the Bean model gives a good approximation for the understanding the the magnetic behavior of type II superconductors.

Bean Approximation

According to this approach, the critical current density is constant inside the superconductor, J_c =ct, which means that it is independent of the magnetic field.

To illustrate this model we consider the magnetization of an infinite cylinder, increasing and decreasing the magnetic field, applied parallel to the cylinder axis, in the Bean critical state model (figure 2.5). These figures show the flux and current distribution inside the cylinder for different applied magnetic fields (H^1, H^* and $2H^*$ increasing magnetic field and H^*, H^1 and H=0 decreasing magnetic field). In the Bean model, J_c is considered to be constant which means that the field gradient within the sample is constant ($\nabla \bigwedge$H=J_c) and, thus, the magnetic field decreases linearly with the distance.

According to the hysteresis loop, when the applied magnetic field increases, flux starts to penetrate inside the superconductor with a constant slope, J_c (2.5a). The field penetration distance, where supercurrents are induced, depends on the applied magnetic field, the sample dimensions and the critical current density. The direction of superconducting currents is indicated in the figure. The total magnetization can be determined from the area limited by the internal magnetic field profiles and the applied magnetic field (shaded zone).

When the applied magnetic field is H^*, the internal magnetic field reaches the center of the sample (see figure 2.5b). This field is called full penetration field. For this value of the applied magnetic field, supercurrents are induced in the whole sample and the associated magnetization saturates (M^{sat}). For an infinite cylinder with radius R, one obtains:

$$J_c = \frac{H^*}{R} \tag{2.3}$$

From the hysteresis loop, the full penetration field can be determined by obtaining the value of applied magnetic field, where the first magnetization curve and the return curve after a complete hysteresis loop merge (see hysteresis loop shown in the figure). For the determination of H^*, one has to apply a maximum

field of H>2H^*. H=2H^* is the minimum value of applied magnetic field needed to saturate the remanent magnetization (see figure 2.5c).

By decreasing the applied magnetic field, the supercurrent flows in an opposite direction (see figure 2.5d). The current direction is determined by the slope of H(r). At this point there is a flux trapped inside the superconductor since internal magnetic field is higher than the magnetic field applied and, thus, the magnetization is positive (M^d). By further decreasing of the applied magnetic field, the supercurrents flowing in opposite direction penetrate inside the sample and the magnetization increases. For an applied field of H^1, the value of magnetization , M^e is almost saturated (figure 2.5e). After having applied a maximum field 2H^*, if the magnetic field is completely removed (H=0), all the supercurrents have changed their direction and the remanent magnetization in the sample is saturated (M^{sat}) (figure 2.5f). If the applied field is lower than 2H^*, the remanent magnetization is smaller than the saturation magnetization, $M^{rem}<M^{sat}$.

When the sample analyzed is of parallelepiped geometry, the critical current density can be determined as follows:

$$J_c^{ab} = \frac{20\Delta M}{a(1-\frac{a}{3b})} \tag{2.4}$$

where ΔM is the width of the saturated hysteresis loop (for $H > 2H^*$), a and b are the dimensions of the transverse section to which the applied magnetic field is perpendicular, a<b.

Bean model, also enables the determination of magnetic field, current and magnetization profiles when a FC process is followed. This means that the superconductor is cooled in the presence of an applied magnetic field. The description is analogous to the description presented for the case of ZFC. In figure 2.6 it is represented the evolution of the magnetization process. In an initial state, the magnetization is zero (figure 2.6a). When the sample is cooled below T_c, a constant magnetic field has penetrated the entire sample. As the external field is decreased, magnetic flux in the surface layers is excluded. The remanent mag-

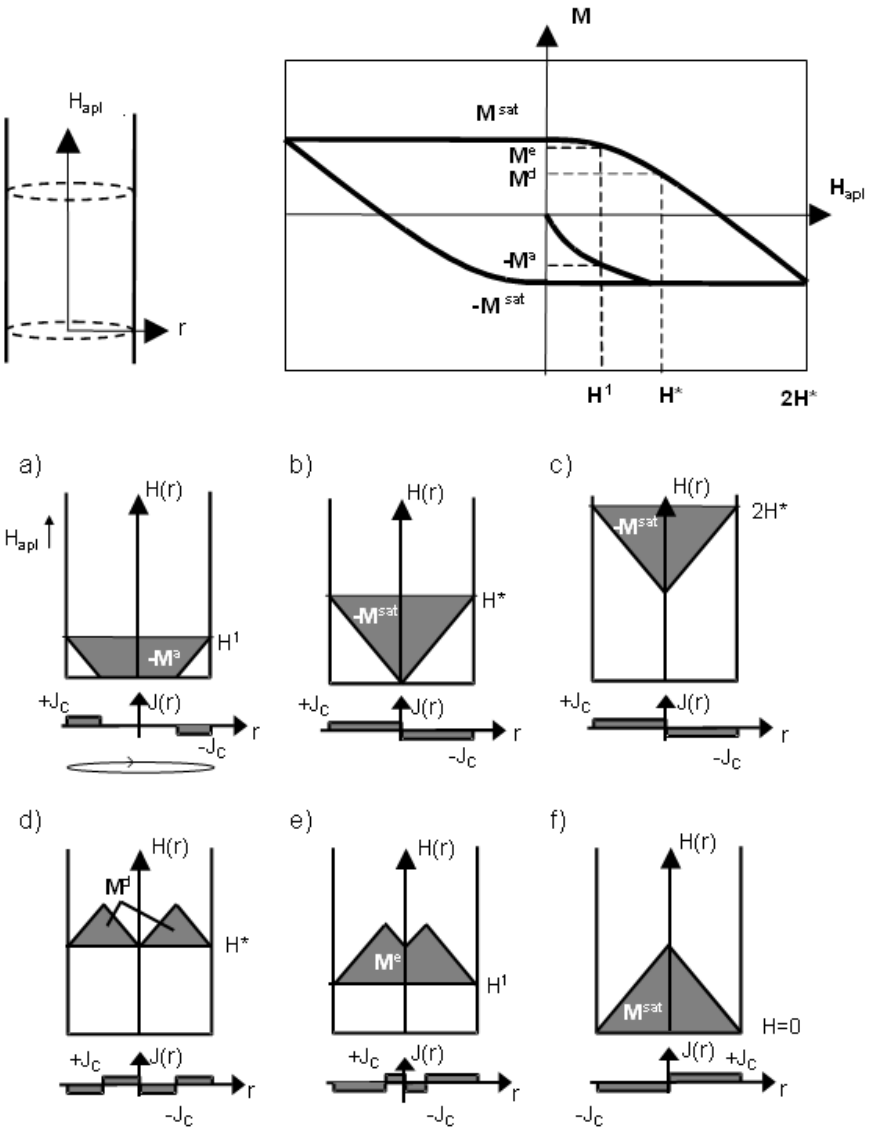

Figure 2.5: Magnetization process for an infinite cylinder based on the Bean critical state model. Schematic representation of magnetic field and current distribution inside the sample. a)-c) increasing the magnetic field; d)-f) decreasing the magnetic field.

netization profile is shown in figure 2.6b. When the applied magnetic field is reduced to zero (H=0), a quantity of flux is trapped inside the superconductor (see figure 2.6c). The shape of the resulting flux profile depends of the field H at which the field-cooled process was performed. If the maximum applied field

was higher than H^*, the remanent magnetization is the saturation magnetization M^{rem}=M^{sat} and the profile of the remanent magnetization is the one presented in figure 2.6c. If this field was smaller than H^*, the remanent magnetization inside the sample is lower than the saturation magnetization M^{rem}<M^{sat} and the remanent magnetization has the profile presented in figure 2.7.

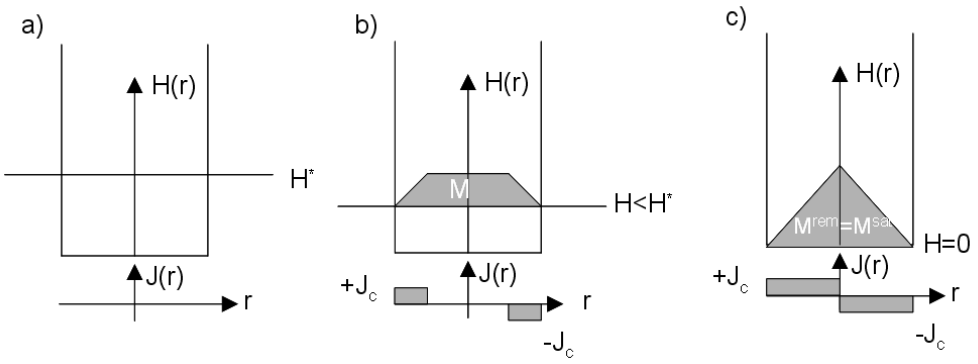

Figure 2.6: Magnetization process for a slab after a fc process. a)initial stage when an magnetic field of H>H^* is applied before the cooling of the sample below its T_c; b) decreasing the applied magnetic field; c) reducing the applied field down to H=0.

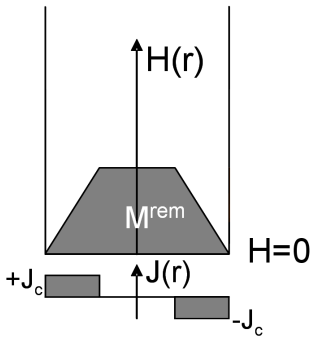

Figure 2.7: Schematic representation of the remanent magnetization profile after a fc process when the applied field is lower than H^*, the full penetration field. In this case the remanent magnetization is lower than the saturated magnetization.

2.1.4 Irreversibility line

The existence of an irreversibility line $H_{irr}(T)$ that lies below H_{c2} on a H versus T phase diagram is an important point to consider for practical applications of high-temperature superconductors (figure 2.8).

In real type II superconductors, zero resistance state is only achieved when flux motion is prevented by pinning centers against the electromagnetic forces. In this case the critical current density is different from 0 (J_c >0) and the vortex state is called irreversible. Between H_{irr}(T) and H_{c2}(T) the superconductor is in the mixed state, but the thermal activation processes are so strong that the material presents a substantial electrical resistance due to flux motion. Therefore, above H_{irr}, the critical current density vanishes to zero (J_c =0) and the vortex state is called reversible.

Thus, the line which separates the reversible from the irreversible state is called irreversibility line and is represented in figure 2.8. For a given material, the material starts to dissipate when the magnetic field applied is H_{irr}(T), called the irreversibility field.

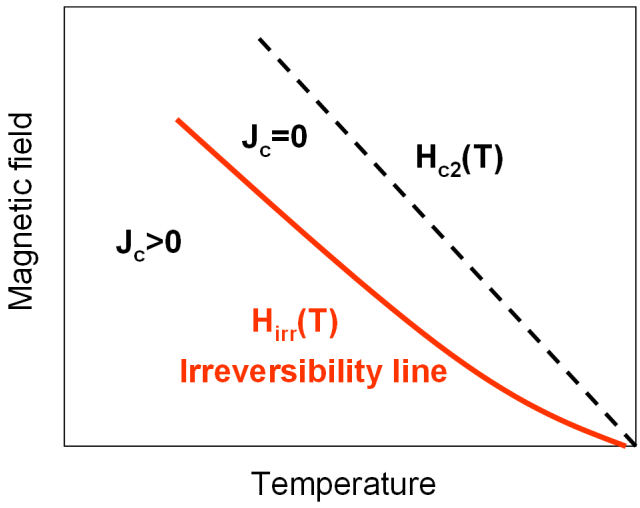

Figure 2.8: Position of irreversibility line $H_{irr}(T)$ in the H-T phase diagram. $H_{irr}(T)$ is below the $H_{c2}(T)$ and divides the states where the critical current density J_c of the superconductor is characterized by J_c =0 and J_c >0.

Since the irreversibility line is below the upper critical magnetic field line (as it can be seen in figure 2.8) the use of these materials at high temperatures and high magnetic fields is limited by $H_{irr}(T)$ (red line in the figure). This line is strongly related to the anisotropy of the cuprates superconductors and it is different for each material as it can be observed in figure 2.9. In this figure are represented H_{irr}(T) lines for different materials: YBCO, Bi and Tl-based materials. YBCO reveals the highest irreversibility fields compared with Tl and Bi compounds. It can be observed that at high magnetic fields, the superconducting properties of Bi and Tl-compunds decrease rapidly. Bi-2223 only can be used for applications which require low magnetic fields H=0.2T if it is to be cooled with liquid nitrogen. Its use at high magnetic fields implies cooling to lower temperatures.

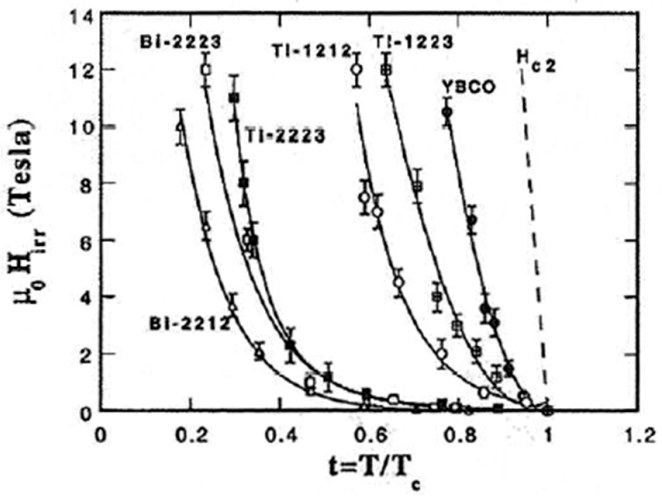

Figure 2.9: The irreversibility line in various cuprates. The dashed line represents the respective H_{c2}.

The YBCO material, on the contrary, keeps its superconducting properties at 77K until a magnetic field of 7-10T is reached. Thus, this material is the most used for the fabrication of rotors for motors who require very high mag-

netic fields. This material has the lower anisotropy of all the high T_c oxides. Its anisotropy is $\simeq$7, whereas the anisotropy of BSCCO is $\simeq$100.

Although BSCCO material have a higher T_c than YBCO material, the superconductor with lower anisotropy and with better performances (higher J_c) at 77K and at high magnetic fields ($\simeq$7-10T) is the YBCO material.

2.2 High-T_c superconductors: $YBa_2Cu_3O_{7-\delta}$ material

The $YBa_2Cu_3O_{7-\delta}$ material was discovered by P. Chu in 1987 and its T_c is $\simeq$91K. Is the first high-T_c superconductor discovered whose critical temperature T_c was above the liquid nitrogen temperature, thus opening the path to many low cost applications.

2.2.1 Crystallographic aspects

The crystallographic structure of high-temperature superconductors (HTS) has been studied since their discovery for many research groups. Crystallographers classify the structure of these oxides as of perovskite type with CuO_2 planes lying normal to the crystallographic c-direction. This is a common feature of these materials, therefore they are often called cuprates.

YBCO exists in either a tetragonal or orthorhombic crystal structure (see figure 2.10), being only superconducting in the orthorhombic phase. The tetragonal phase is observed at high temperatures in a range between 750°C and 900°C. On decreasing the temperature and increasing the oxygen content of the sample, by oxygen uptake and diffusion, a second-order phase transition occurs at about 700°C from the tetragonal to the orthorhombic phase.

As shown in figure 2.10 the orthorhombic structure of YBCO can be schematically represented as a layered structure where three planes consisting in Cu and O atoms are intercalated with two planes containing Ba and O and one plane containing Y. In the tetragonal phase (figure 2.10a), the oxygen sites in the basal plane are about half occupied in the random manner, while in the orthorhombic

phase (figure 2.10b) they are ordered into Cu-O chains along the b-direction. The oxygen vacancies along the a-direction in the orthorhombic phase cause the unit cell to compress slightly so that $a < b$. In the orthorhombic phase, both, the CuO_2 planes and the Cu-O chains, contribute to the superconductivity; the CuO_2 planes contain mobile charge carriers (holes), and the Cu-O chains act as charge reservoirs that transfer holes to the planes.

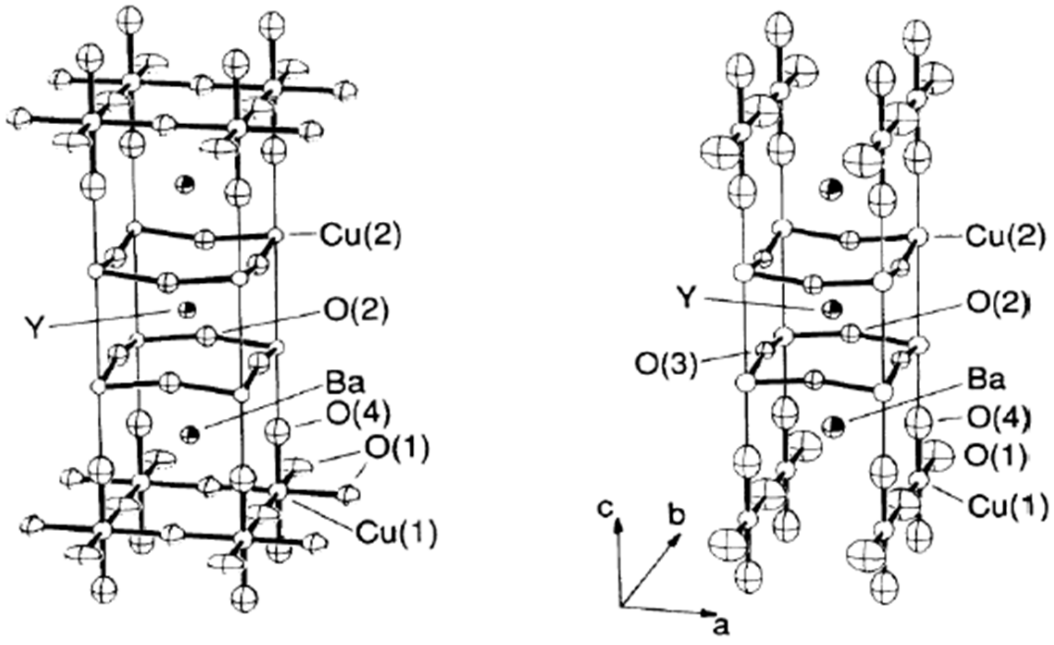

Figure 2.10: Sketches of the unit cell of the a)tetragonal and b)orthorhombic phases of YBCO [23]. Representative lattice parameters for the orthorhombic phase are a=3.827$\mathring{A}$, b=3.882$\mathring{A}$ and c=11.682$\mathring{A}$.

The oxygen content in YBCO determines the crystallographic structure (figure 2.11a) and the hole concentration in the CuO_2 planes. For an oxygen content x=6 (where x=7-δ), the compound $YBa_2Cu_3O_6$ is in the tetragonal phase and it is an insulator. Increasing the oxygen content up to x=6.6, the compound undergoes a phase transition from tetragonal to orthorhombic. Finally, raising x to 6.94, T_c approaches its maximum value (93K). Above x=6.94, T_c drops by about 4K

(see figure 2.11b). The maximum value found for T_c is due to an optimal hole doping of CuO_2 planes. The drop of T_c, when x exceeds 6.94, has been explained as being in overdoped state, when the holes in CuO_2 planes exceed the optimum concentration.

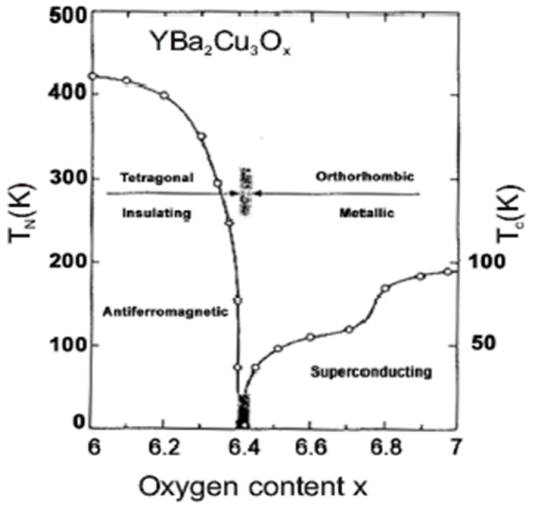

(a)

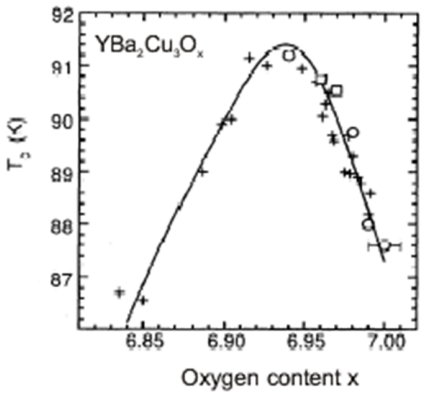

(b)

Figure 2.11: a) Phase diagram of $YBa_2Cu_3O_{7-\delta}$ system as a function of oxygen content. T_N represents the Niel temperature of the antiferromagnetic phase and T_c the critical temperature of the superconducting phase. b) Variation of T_c with oxygen content.

2.2.2 Anisotropy of YBCO material

Another important aspect of $YBa_2Cu_3O_{7-\delta}$ material is that, like the other cuprates, has an anisotropic behavior, as a consequence of its crystalline structure that is reflected in the directional dependence of λ, ξ and H_{c2}. The anisotropy of these parameters is remarkable between the c-direction and the a or b direction, while the anisotropy between the a and b directions is small and can be neglected in most cases. The anisotropy of HTS materials can be described using Ginzburg-Landau theory that introduces a different effective mass of the hole carriers in different directions. The effective mass in the ab plane is denoted m_{ab} and along the c-axis m_c. The anisotropy is described by the parameter γ, defined as γ=$(m_c/m_{ab})^{1/2}$=λ_c/λ_{ab}=ξ_{ab}/ξ_c=H_{c2}^{ab}/H_{c2}^{c} [24, 25] with γ>1. The value for YBCO lies between 5 and 8 [26], while in $Tl_2Ba_2CaCu_2O_x$ γ was found to be $\approx$ 90 [27] and in $Bi_2Sr_2CaCu_2O_x$ it exceeds 150 [28]. The large γ values of Tl and Bi compounds indicate a high anisotropy. On the contrary, YBCO has a relatively small γ value which means that it is less anisotropic.

The anisotropy of high-T_c superconductors is related to their layered structure and long separation between the CuO_2 planes when compared to ξ_c. YBCO is the less anisotropic high-T_c superconductor because on one side the distance between CuO_2 planes is only d$\approx$8$\mathring{A}$ and on the other side the CuO chains have metallic conductivity and the superconductivity is induced by proximity effect. In contrast, Bi, Tl and Hg compounds are more anisotropic because the charge reservoir blocks are insulators and the distance is much larger than the respective value of 2ξ_c. The anisotropy of the effective mass γ in these compounds drive, as a consequence, to an anisotropy in the critical current density, i.e. $J_c^{ab}>>J_c^{c}$.